ACI STRUCTURAL JOURNAL TECHNICAL PAPER

Title no. 107-S14

Shear Behavior of Headed Anchors with Large Diameters and Deep Embedments

by Nam Ho Lee, Kwang Ryeon Park, and Yong Pyo Suh

This paper presents shear test results for large cast-in-place anchor bolts in concrete. The tests were performed to evaluate the shear performance of large anchors, that is, anchors with a diameter greater than 2 in. (50.8 mm) or an embedment depth greater than 25 in. (635.0 mm), which are not addressed by ACI 318-08, Appendix D and ACI 349-06, Appendix D. The tests were also intended to investigate the safety of such anchors for use in nuclear power plants, and the effects of regular (conventional) and special reinforcement on the shear strength of such anchors. The test results are used to assess the applicability of existing design formulas valid for smaller anchors to large anchors. Suggestions are made for incorporating the effects of deep embedment or large diameter in existing design provisions for cast-in-place anchor bolts under shear load.

Keywords: anchor; anchor bolt; cast-in-place; embedments; shear tests.

INTRODUCTION

Current anchorage designs for nuclear power plants in Korea use large anchor bolts with diameters exceeding 2 in. (50.8 mm), embedment depths exceeding 25 in. (635.0 mm), a specified yield strength of 140 ksi (980.0 MPa), and a specified ultimate strength of 155 ksi (1085.0 MPa). While the shear behavior of anchors up to approximately 1 in. (25.4 mm), whose ultimate strength is governed by concrete edge breakout has been studied extensively,[1,2] large anchors installed near edge have not been adequately addressed. In the research described herein, large anchors installed near edge were tested in shear to develop design criteria for anchors that are not addressed by ACI 318-08 Appendix D[3] or ACI 349-06 Appendix D,[4] and to evaluate the applicability to large anchors of predictive equations for concrete edge breakout developed for smaller anchors.

To evaluate the shear behavior of anchors with large diameters and embedment depths at various edge distances, anchors with diameters of 2.5, 3.0, and 3.5 in. (63.5, 76.2, and 88.9 mm), embedment depths of 25, 30, and 35 in. (635.0, 762.0, and 889.0 mm) and an edge distance of 15, 20, and 30 in. (381.0, 508.0, and 762.0 mm) were tested. In addition, several reinforcement patterns were arranged for 2.0 in. (50.8 mm) diameter anchors with 25 in. (635.0 mm) embedment depths and 15 in. (381.0 mm) edge distances to evaluate the effectiveness of reinforcement for increasing the shear capacity and ductility of near-edge anchors.

RESEARCH SIGNIFICANCE

The research described herein is, to the authors' knowledge, the first experimental information on the shear behavior of very large headed anchor bolts ($d_o \geq 2$ in. [50.8 mm], $h_{ef} \geq 21$ in. [525.0 mm]). It is significant because although such anchor bolts are commonly used, for example, in power plants and for the anchorage of tanks, design provisions validated by the test do not currently exist.

EXISTING FORMULAS FOR PREDICTING SHEAR CAPACITY OF ANCHOR IN CONCRETE AS GOVERNED BY CONCRETE EDGE BREAKOUT

Expressions currently used for computation of the concrete edge breakout strength of shear loaded anchor bolts are given by Eq. (1) through (4). The concrete edge breakout provisions of ACI 318-08[3] and ACI 349-06[4] are based on the Concrete Capacity Design approach (CCD method) (Fuchs et al.)[1]. The presence of reinforcement is not taken into consideration by the aforementioned provisions.

Equations (1) and (2), which are associated with the CCD method[1] and the Modified CCD method,[2] respectively, are based on the mean concrete breakout capacity in uncracked concrete. In contrast, Eq. (3) of ACI 349-97[5] is based on a lower bound value of test results, and Eq. (4) of ACI 349-06 is based on the 5% fractile of tested shear breakout capacities, but both are assumed to be based on 5% fractile values in this paper. Therefore, while the extrapolated mean shear breakout capacities computed by Eq. (1) and (2) were compared with the measured mean capacities, the capacities calculated by Eq. (3) and (4) are compared with the 5% fractile values of the measured capacities. Equations (1) and (2) were developed in SI units. Equation (1) was converted into lb-in. units for comparison with other methods. Equation (2), which was developed in SI units, is not readily convertible to lb-in. units. A ratio of 5% fractile-to-mean value of 0.75 is assumed in ACI 349-06 (refer Eq. (1) and (4)). For ACI 349-06, the value $k = 7$ is valid for cracked concrete but the tests were performed in uncracked concrete. Assuming a ratio of uncracked to cracked strength of 1.4, a value $k = 9.8$ ($k = 7 \times 1.4$) was used for the calculation of predicted capacities. The purpose of this computation is to test the applicability of the expressions to large anchors

CCD method (in U.S. Customary Units):

$$V_n = 13\left(\frac{\ell}{d_o}\right)^{0.2}\sqrt{d_o}\sqrt{f_c'}(c_1)^{1.5} \quad \text{(lb)} \qquad (1)$$

Modified CCD method (in SI Units):

$$V_n = 3d_o^{0.1(h_{ef}/c_1)^{0.5}} h_{ef}^{0.1(d_o/c_1)0.2}\sqrt{f_{cc}'}(c_1)^{1.5} \quad \text{(N)} \qquad (2)$$

ACI Structural Journal, V. 107, No. 2, March-April 2010.
MS No. S-2008-238 received July 16, 2008, and reviewed under Institute publication policies. Pertinent discussion including author's closure, if any, will be published in the January-February 2011 *ACI Structural Journal* if the discussion is received by September 1, 2010.

ACI member **Nam Ho Lee** *is a Senior Engineer at Atomic Energy of Canada Limited (AECL). He received his BS from Seoul National University, Seoul, Korea, and his MS and PhD from Korea Advanced Institute of Science & Technology, Daejeon, Korea. He is a member of ACI Committees 349, Concrete Nuclear Structures; 355, Anchorage to Concrete; and Joint ACI-ASCE Committee 359, Concrete Components for Nuclear Reactors. His research interests include nonlinear behavior of concrete structures, aircraft impact on concrete structures, and anchorage to concrete.*

Kwang Ryeon Park *is a Senior Research Engineer in the Civil Engineering Department of the Korea Power Engineering Company. His research interests include post-installed and cast-in anchorage to concrete.*

Yong Pyo Suh *is a Principal Researcher at Nuclear Power Laboratory, Korea Electric Power Research Institute, Daejeon, Korea. His research interests include the behavior of concrete-filled steel plate structures and anchorage to concrete.*

ACI 349-97 (45-Degree Cone Method) (in U.S. Customary Units):

$$V_b = 2\pi\sqrt{f_c'}(c_1)^2 \quad \text{(lb)} \tag{3}$$

ACI 349-06 (in U.S. Customary Units):

$$V_b = 9.8\left(\frac{\ell}{d_o}\right)^{0.2}\sqrt{d_o}\sqrt{f_c'}(c_1)^{1.5} \quad \text{(lb)} \tag{4}$$

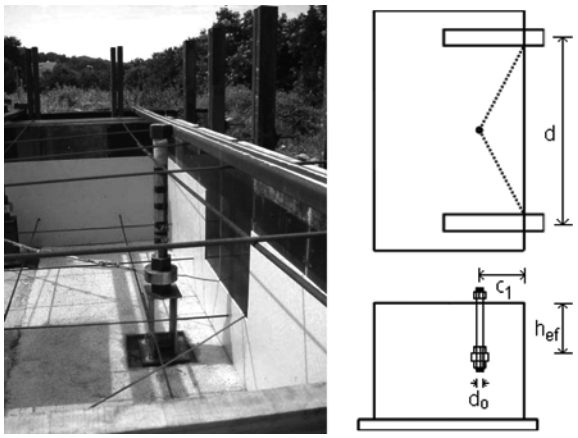

Fig. 1—Schematic sketch and photo of Specimens S1 to S7. (Dimensions of d, h_{ef}, c_1, *and* d_o *for each specimen are shown in Table 1.)*

where f_c' is concrete compressive strength (psi) to be verified using cylinders; f_{cc}' is concrete compressive strength (MPa) to be verified using 200 mm (7.87 in.) cubes; h_{ef} is embedment depth (mm for Eq. (2) and in. for other equations); d_o is diameter of anchor (mm for Eq. (2) and in. for other equations); ℓ is load bearing length of anchor (in.); and c_1 is anchor edge distance (mm for Eq. (2) and in. for other equations).

EXPERIMENTAL PROGRAM

Test specimens

The test program is summarized in Table 1, and the specimens with and without supplementary reinforcements are shown in Fig. 1 and 2, respectively. Test groups VD and VH are intended to examine the effect of anchor diameter and embedment depth on the shear breakout strength of anchors without supplementary reinforcement. Specimen S5, with an embedment depth of 35 in. (889.0 mm) deeper than those of Specimens S2 and S4, was planned but not tested because Specimens S2 and S4 showed that the shear breakout capacities were not influenced by embedment depth. Test group VE was planned to examine the effects of edge distance on unreinforced concrete shear breakout strength. Test group VR was intended to examine the effects of different arrangements of supplementary reinforcement with a relatively short edge distance.

To evaluate the effects of edge distance, embedment depth, anchor diameter, and supplementary reinforcement patterns on the shear capacity of large anchors, nine different test configurations were selected. Five test replicates with one each of test Specimen S1 to S4, four replicates of Specimen S6, and three replicates of Specimen S7 were performed for a total of 27 tests on anchors without supplementary reinforcement. Three replicates of test Specimen S8, S9, and S10 and one replicate of Specimen S9-1 and S9-2 were also performed for a total of 11 tests with various patterns of supplementary reinforcement.

All anchors were fabricated with ASTM A540 Grade B23 Class 2 steel (equivalent to ASME SA 549 Grade B23 Class 2 used in Korean nuclear power plants) with f_y = 140 ksi (980.0 MPa) and f_u = 155 ksi (1085.0 MPa). The anchor head consisted of a round thick plate that was fixed to the threaded end of the bolt with clamping nuts (Fig. 3). The bearing plates were provided to match the specimens used in a companion study[6] to investigate the tension capacity of large anchors. The steel plate (ASTM A36) provides a

Table 1—Description of shear test specimens

Test group		Specimen (no. of replicates)	Supplementary reinforcement	Anchor diameter d_o, in. (mm)	Effective embedment h_{ef}, in. (mm)	Clear distance d, in. (mm)	Edge distance c_1, in. (mm)
VD	VD1	S1(5)	None	2.5 (63.5)	25 (635.0)	81.2 (2062.5)	20 (508.0)
	VD2	S2(5)	None	3.0 (76.2)	25 (635.0)	81.2 (2062.5)	20 (508.0)
	VD3	S3(5)	None	3.5 (88.9)	25 (635.0)	81.2 (2062.5)	20 (508.0)
VH	VH1	S2(5)	None	3.0 (76.2)	25 (635.0)	81.2 (2062.5)	20 (508.0)
	VH2	S4(5)	None	3.0 (76.2)	30 (762.0)	81.2 (2062.5)	20 (508.0)
	VH3	S5(0)	None	3.0 (76.2)	35 (889.0)	Not tested	20 (508.0)
VE	VE1	S6(4)	None	2.5 (63.5)	25 (635.0)	63.8 (1620.5)	15 (381.0)
	VE2	S7(3)	None	2.5 (63.5)	25 (635.0)	151.2 (3840.5)	30 (762.0)
	VE3	S1(5)	None	2.5 (63.5)	25 (635.0)	81.2 (2062.5)	20 (508.0)
VR	VR1	S8(4)	Fig. 2	2.5 (63.5)	25 (635.0)	63.8 (1620.5)	15 (381.0)
	VR2	S9(4)	Fig. 2	2.5 (63.5)	25 (635.0)	63.8 (1620.5)	15 (381.0)
	VR3	S10(4)	Fig. 2	2.5 (63.5)	25 (635.0)	63.8 (1620.5)	15 (381.0)
	VR4	S6(4)	None	2.5 (63.5)	25 (635.0)	63.8 (1620.5)	15 (381.0)

Note: Refer to Fig. 1 for notation of d, h_{ef}, c_1, and d_o.

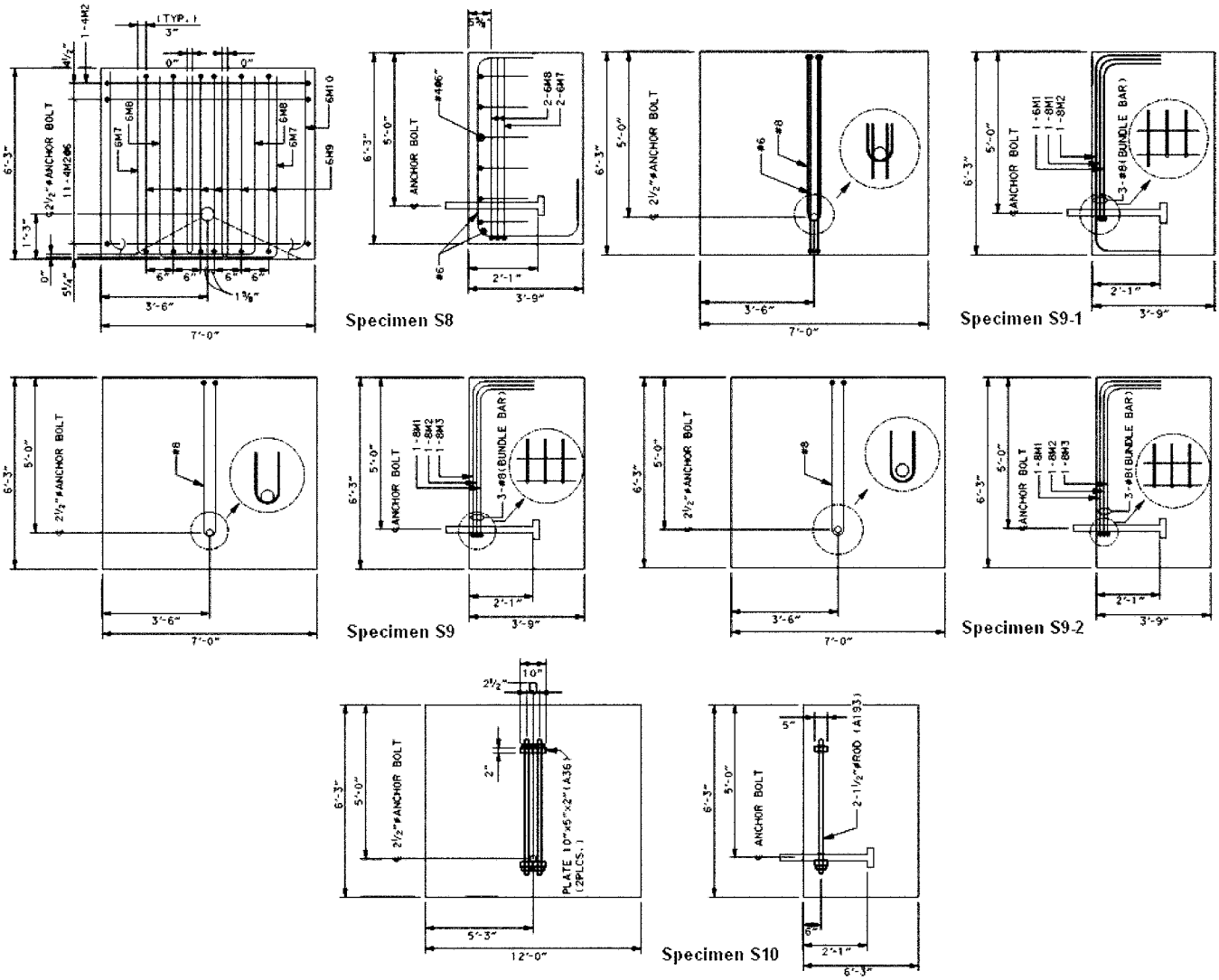

Fig. 2—Schematic sketches of Specimens S8 to S10. (Note: 1 ft = 0.305 m; 1 in. = 25.4 mm.)

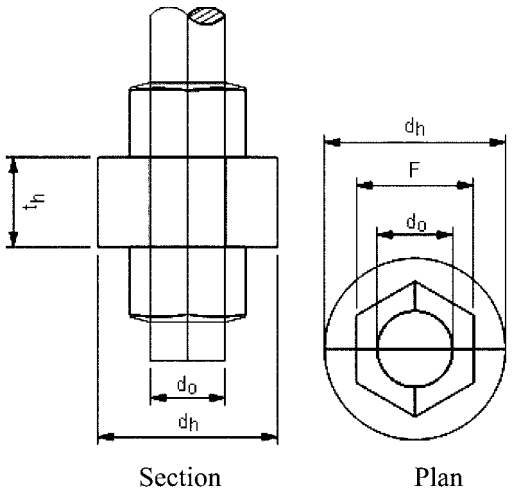

Anchor Dia. d_o, in.(mm)	Plate Dia. d_h, in.(mm)	Plate thick. t_h, in.(mm)	Nut width F, in.(mm)
2.5(63.5)	6.0(152.4)	2-1/2(63.5)	3-7/8(98.4)
3.0(76.2)	7.0(177.8)	3.0(76.2)	4-5/8(117.5)
3.5(88.9)	9.0(228.6)	4.0(101.6)	5-3/8(136.5)

Fig. 3—Details of anchor head.

Table 2—Concrete mixture proportions

Nominal strength, psi (MPa) at 42 days	W/ (C+FA)	S/a, %	W, lb	C, lb	FA, lb	S, lb	G, lb	WRA,* mL	AE,† mL
5500 (38.0)	0.44	44	285	514	128	1257	1617	474	26

*Water-reducing admixture.
†Air-entraining admixture.
Note: 1 lb = 0.4536 kg; 1 mL = 0.034 oz.

minimum net bearing area satisfying the pullout strength requirement of Eq. (D-15) of ACI 349-06 Appendix D[4] for each anchor bolt. The nominal strength of the anchor bolt was conservatively used as the pullout strength N_p for each specimen. Refer to Fig. 3 for the dimensions of the bearing plates.

The size of the concrete test block was considered to be large enough to avoid splitting failure. The clear distance for each anchor is provided to be free from the effect of test loading frame supports (refer to Table 1). As shown in Fig. 1, wooden and steel frames were constructed to suspend the cast-in-place anchors in the correct position and at the correct embedment depth. These wooden and steel frames were removed after curing the concrete test block.

The concrete mixture for the test specimens is shown in Table 2. The concrete used in the test specimens was comparable to the concrete used in Korean nuclear power plants, except that 20% by weight of Type I cement was substituted with fly ash and 1 in. (25.4 mm) crushed aggregate was used instead of 3/4 in. (19.0 mm). The specified 28-day concrete strength was f_c' = 5500 psi (38.0 MPa). Actual concrete compressive strengths of test specimens at the time of testing are, on average, f_c' = 5652 psi (38.969 MPa). The concrete for the specimens of each test series was poured from a single batch.

Supplementary reinforcement in the S8 test blocks was placed orthogonally at the top face and vertically at the front (edge) face. The anchors in the S9 blocks were enclosed by three No. 8 U-shaped hairpins with hooked tails placed in contact with the anchor. Specimen S9-1 was reinforced with two No. 8 U-shaped hairpins and two No. 6 conventional hooked bars placed beside the anchor. Specimen S9-2 was enclosed by three No. 8 U-shaped hairpins close to but not in contact with the anchor. Each anchor of Specimen S10 was enclosed by two 1-1/2 in. (38.0 mm) rods with plates 10 x 5 x 2 in. (254.0 x 127.0 x 50.8 mm) (A36). Refer to Fig. 2 for the details of supplementary reinforcements.

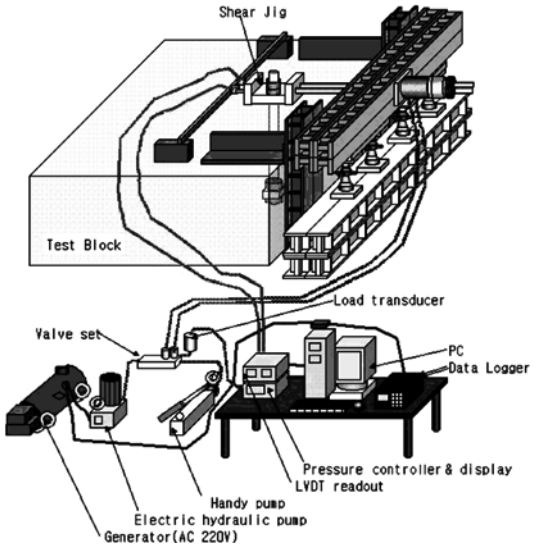

Fig. 4—Schematic of shear test setup.

The supplementary reinforcement was designed to take up the shear steel capacity of the anchor (456 kips [2031.0 kN]). The supplementary No. 8 U-shaped hairpins were fabricated with $6d_b$ bend diameter and located at a cover depth of 2 in. (50.0 mm) from the surface of the concrete.[4]

Test setup

The test setup consisted of a loading frame, loading plate, jack assembly, and load cell, as shown in Fig. 4. The load was applied to the anchor under force control in increasing percentages of the estimated capacity (5%, 10%, 20%, and so forth to failure) with loading frames oriented parallel to the concrete surface of each specimen. Loads were continuously and very slowly increased to avoid abrupt failure and displacements were observed at the increments in the range of approximately 2.5% to 5% of predicted peak load, that is, observed at every increment of approximately 5.5 to 11 kips (24.5 to 49.0 kN) for 5 to 10 minutes depending on magnitude of the applied load at each observation step. The clear distance between the supports was $4.0c_1$ for Specimen S1 through S9, allowing for unrestricted formation of a concrete breakout. Test data included applied load (measured by a load cell); the displacement of the anchor in the direction of load at the level of concrete top surface (measured by an LVDT at the center of the jig plate, Fig. 4); and axial strains in the anchor bolt, the supplementary reinforcement, or both.

TEST RESULTS

Peak loads, failure modes at peak loads, and load-displacement behavior

The average failure loads for the unreinforced and the reinforced shear test specimens are summarized by edge distances, anchor diameters, and effective embedment depths in Table 3 and 4, respectively. The values are normalized to f_c' = 5500 psi (38.0 MPa) by multiplying the measured peak load of each test by the ratio $\sqrt{5500/f'_{c,\,actual}}$. In Tables 3 and 4, the measured mean capacities are compared with the values predicted by the CCD method and the Modified CCD method, and the 5% fractile capacities are compared with the prediction according to ACI 349-97 and ACI 349-06. The

Table 3—Tested and predicted shear capacities for Specimens S1 to S7

Classification	Reference	Concrete shear breakout capacities, kips (kN) ($d_o/h_{ef}/c_1$)					
		S1 2.5/25/20	S2 3.0/25/20	S3 3.5/25/20	S4 3.0/30/20	S6 2.5/25/15	S7 2.5/25/30
Predictions	CCD method, Eq. (1)	216 (961)	228 (1014)	239 (1063)	237 (1054)	140 (623)	397 (1766)
	Modified CCD method Eq. (2)	126 (560)	130 (578)	135 (600)	138 (614)	90 (400)	205 (912)
	ACI 349-97, Eq. (3)	186 (827)	186 (827)	186 (827)	186 (827)	105 (467)	419 (1864)
	ACI 349-06, Eq. (4)	163 (725)	172 (765)	180 (801)	178 (791.8)	106 (471.5)	299 (1330)
Tests	Mean	107.6 (479)	98.9 (440)	103.5 (460)	99.9 (444)	60.0 (267)	242 (1077)
	COV, %	1.9	4.6	5.7	4.4	4.6	2.5
	5% fractile	100.8 (448)	83.3 (371)	83.4 (371)	84.9 (378)	48.8 (217)	209.7 (933)
	5% fractile/mean	0.94	0.84	0.81	0.85	0.81	0.87

Classification	Comparison	Ratio of tested to predicted capacity						
		S1	S2	S3	S4	S6	S7	Mean
Mean of test results	Mean/Eq. (1)	0.50	0.43	0.43	0.42	0.43	0.61	0.47
	Mean/Eq. (2)	0.85	0.76	0.77	0.72	0.67	1.18	0.83
5% fractile of test results	$V_{n,5\%}$/Eq. (3)	0.54	0.45	0.45	0.46	0.46	0.50	0.48
	$V_{n,5\%}$/Eq. (4)	0.62	0.48	0.46	0.48	0.46	0.70	0.53

Table 4—Test results for Specimens S8 to S10 with same parameters as Specimen S6

Classification	Reference	Concrete breakout capacities in kips (kN) with edge distance, 15 in. (381 mm); anchor diameter, 2.5 in. (63.5 mm); and embedment depth, 25.0 in. (635 mm)			
		S8	S9	S10	S6
Predictions (no supplementary reinforcement)	CCD, Eq. (1)	140.0 (622.7)	140.0 (622.7)	140.0 (622.7)	140.0 (622.7)
	Modified CCD, Eq. (2)	90.0 (400.3)	90.0 (400.3)	90.0 (400.3)	90.0 (400.3)
	ACI 349-97, Eq. (3)	105.0 (467.0)	105.0 (467.0)	105.0 (467.0)	105.0 (467.0)
	ACI 349-06, Eq. (4)	106.0 (471.5)	106.0 (471.5)	106.0 (471.5)	106.0 (471.5)
Tests	Mean	202.2 (899.0)	146.4 (651.0)	109.1 (485.0)	60.0 (267.0)
	COV, %	5.5	16.2	17.6	4.6
	5% fractile	158.3 (704.0)	52.6 (234.0)	33.2 (147.0)	48.8 (217.0)
	5% fractile/mean	0.78	0.36	0.30	0.81

Classification	Comparison	Ratios of observed to predicted capacities				
		S8	S9	S10	S6	S8/S6
Mean of test results	Mean/Eq. (1)	1.44	1.05	0.78	0.43	3.35
	Mean/Eq. (2)	2.25	1.63	1.21	0.67	3.36
5% fractile of test results	$V_{n,5\%}$/Eq. (3)	1.51	0.50	0.32	0.46	3.28
	$V_{n,5\%}$/Eq. (4)	1.49	0.50	0.31	0.46	3.24

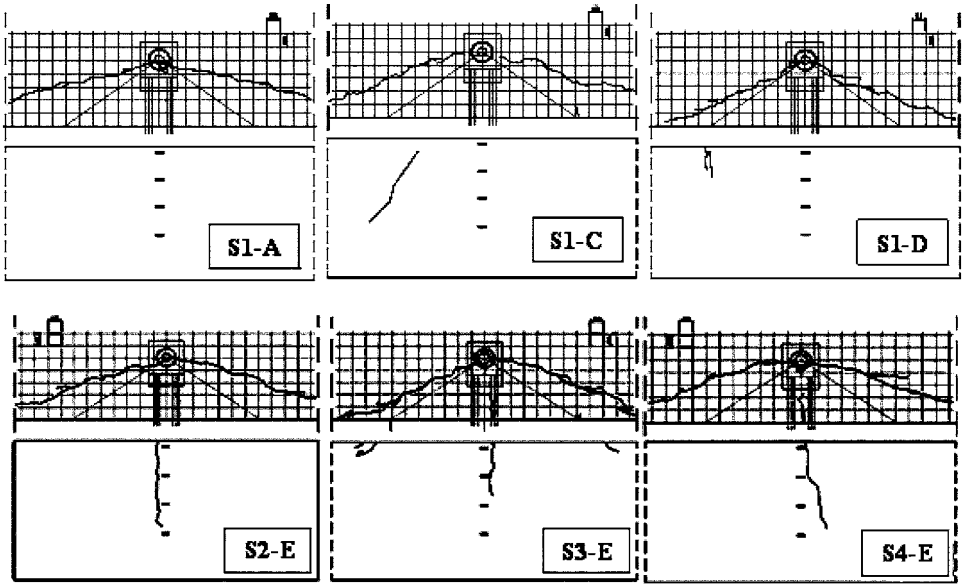

Fig. 5—Typical crack pattern of test specimens.

5% fractile was calculated assuming an unknown standard deviation and a 90% confidence.

Specimens S1 through S7 failed by concrete edge breakout at peak loads below the concrete shear breakout capacities predicted by Eq. (1) to (4) (refer to Table 3). The typical cracking patterns mapped on the grid size of 4 x 4 in. (101.6 x 101.6 mm) of the front face (edge face) and top face of test specimens and typical crack pattern of specimens without supplementary reinforcements are depicted in Fig. 5. The general cracking pattern comprised one major longitudinal crack centered approximately on the front face of the block with inclined cracks on the sides of the front face (edge face), as typically shown in Fig. 5. Crushing of the concrete in front of the anchor was not observed in the tests.

On the top surface, the cracks generally formed an edge breakout failure pattern with breakout prism angles of approximately 15 to 25 degrees initiating at the anchor bolt. Some replicates of Specimens S3, S4, and S7 (without supplementary reinforcement) showed cracks normal to the edge emanating from the anchor; such cracks were judged to have

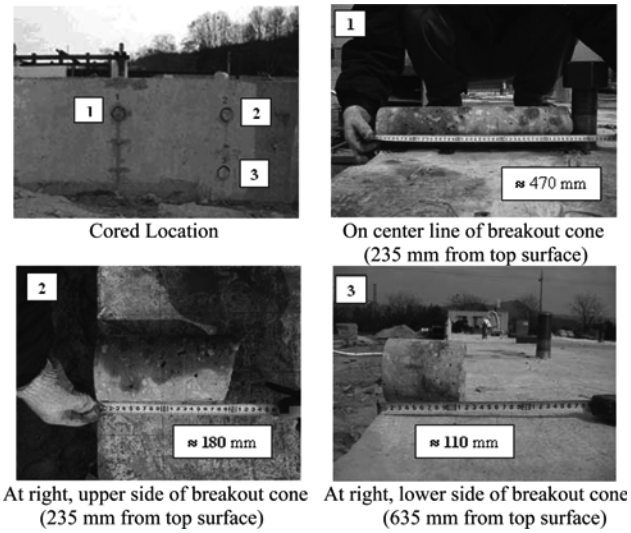

Fig. 6—Internal crack profile in Specimen S1. (Note: 1 mm = 0.0394 in.)

developed due to the flexural behavior of a part of an edge breakout (partly separated from the main test block by edge breakout failure) having two end supports. To physically identify the internal crack propagation defining the concrete breakout failure, one replicate of Specimen S1 was selected, and the concrete was cored from the front face, as shown in Fig. 6.

In four of the replicates of Specimen S6, major cracks had propagated to the midpoint of the eventual concrete edge breakout crack at peak load and almost no cracking was visible on the front face (edge). An exception to this behavior was noted in the case of Specimen S6-D. This may be because the shear load was not transferred along the entire embedment length due to the proximity of the anchor to the edge (15 in. [381.0 mm]); the concrete breakout occurred at a peak load of approximately 60 kips (267.0 kN).

Three replicates of Specimen S7 exhibited cracks at approximately 50% of the ultimate test load, approximately 110 kips (489.0 kN). These cracks extended approximately 5 in.

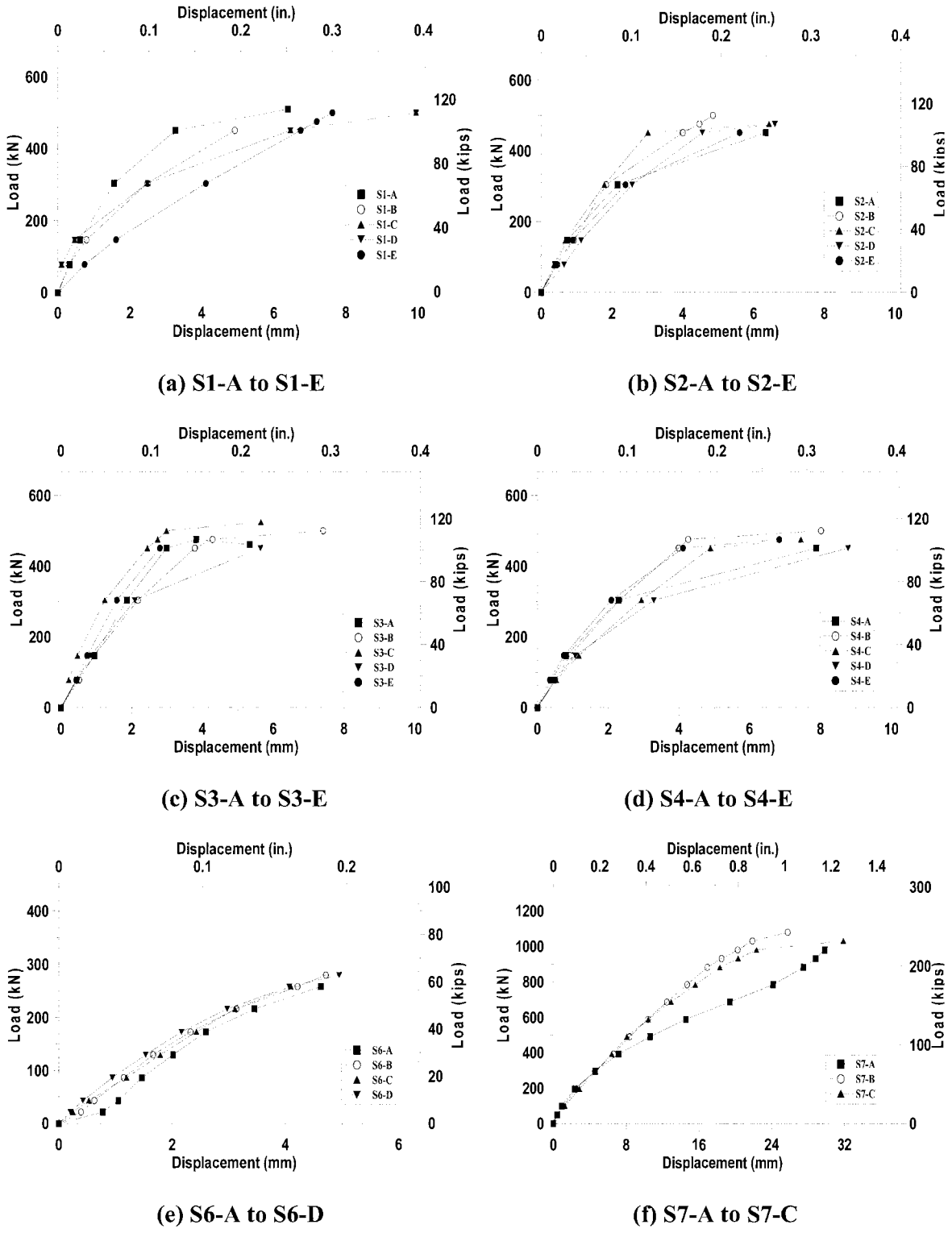

Fig. 7—Measured load-displacement relationships (no supplementary reinforcement).

(127.0 mm), or roughly twice the anchor diameter from the anchor toward the free edge. Cracks extending from the anchor and normal to free edge appeared at approximately 60% (140 kips [623.0 kN]) of the ultimate test load and propagated to the edge with increasing test load. One replicate of Specimen S7, in an anchor located at one edge of the test block, failed in flexure prior to shear breakout failure. The flexural failure was estimated to have occurred because of the location of the specimen at the edge without adequate area to prevent failure due to bending.

The tests of Specimens S8, S9, and S10 did not achieve a failure corresponding to yield strength of supplementary reinforcement because of limitations in the stroke of the loading ram (refer to Table 4). Based on a review of the load-displacement curves, however, it was judged that the possible increase in failure load was not to be high considering the anchor's displacement permissible generally to attachments such as the equipment/system anchored to the concrete structure in the nuclear power plant.

Specimen S8, with supplementary reinforcement consisting of hooked bars and U-shaped stirrups, shows a half pyramid-shaped crack with angles close to 35 degrees, unlike those observed in the specimens without supplementary reinforcement. It also shows that many cracks appeared around the anchor bolt and some bell-shaped cracks or vertical crack lines on the face of the edge. This typical crack pattern is believed to be due to the arrangement of the supplementary reinforcement at the top surface.

Specimen S9 shows top-surface crack patterns similar to those of Specimen S6 (no supplementary reinforcement), except for some cracks along the front face (edge). The test loads required to initiate cracks were approximately 1.5 to 1.7 times the failure loads for Specimen S6, while the ultimate test load for Specimen S9 is approximately 2 to 2.5 times those of Specimen S6. The anchor reinforced by a hairpin bent in a U-shape developed more shear capacity than those in unreinforced concrete. Specimen S10 shows crack patterns with many cracks in a cone shaped breakout, which are different from those for other specimens. Cracks were initiated at a test load closer in magnitude to those for unreinforced Specimen S6.

The load-displacement curves for Specimens S1 through S7 (no supplementary reinforcement) and for Specimens S8 through S10 (supplementary reinforcement) are shown in Fig. 7 and 8, respectively, using the displacement measured at the center of the jig plate. The load-displacement relationship for each test replicate varied based on the concrete strength at the time of testing. Because all specimens failed by concrete breakout prior to yielding of the anchor steel, the total deformations consist almost completely of concrete deformation.

Comparison of predicted and tested shear breakout capacities

The predicted shear breakout capacities ($N_{predicted}$) and the mean and 5% fractile of tested capacities (N_{tested}) are presented in Tables 3 and 4. For Eq. (2), a conversion factor of 1.18 was assumed for the ratio of the cube strength to cylinder strength. In addition, the value of shear bearing length was taken equal to h_{ef} in all expressions. Results for each replicate were normalized by the square root of compressive capacity at test age. Predicted shear capacities of ACI 349-06 and ACI 349-97 are based on and assumed to be based on the 5% fractile, respectively, as previously mentioned, while those for the CCD methods are based on the mean of the test results. Corresponding experimental values are used for comparison. In Fig. 9, the peak loads

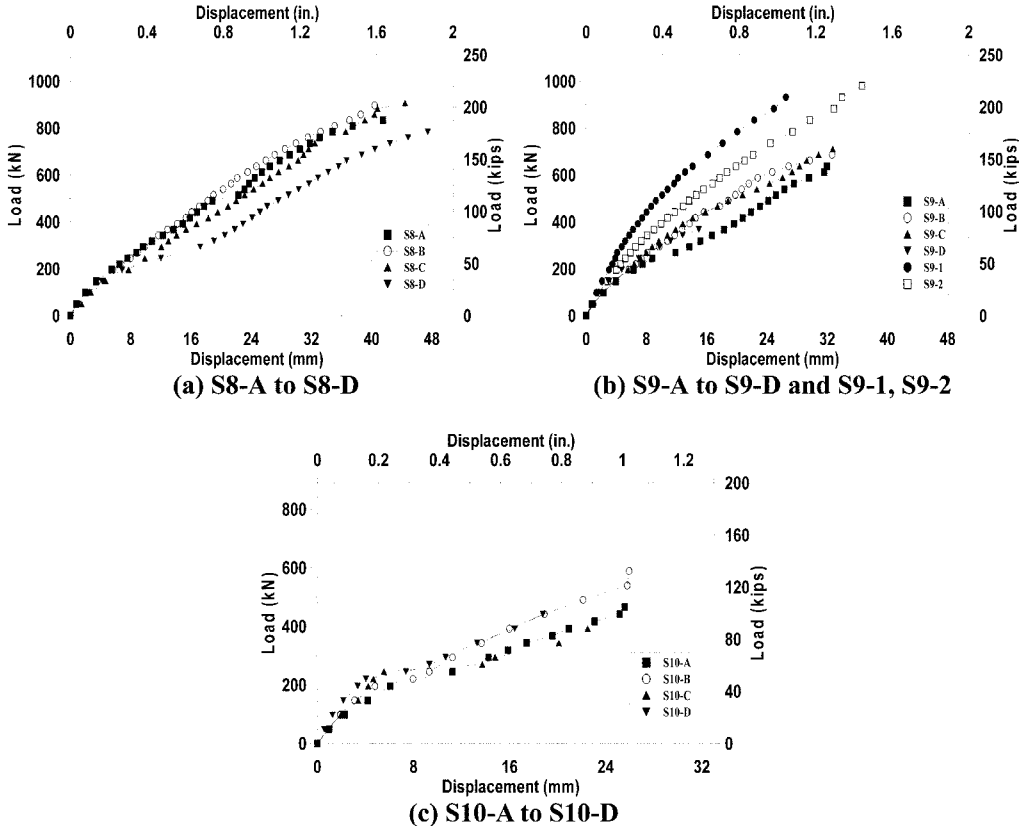

Fig. 8—Measured load-displacement relationships (supplementary reinforcement).

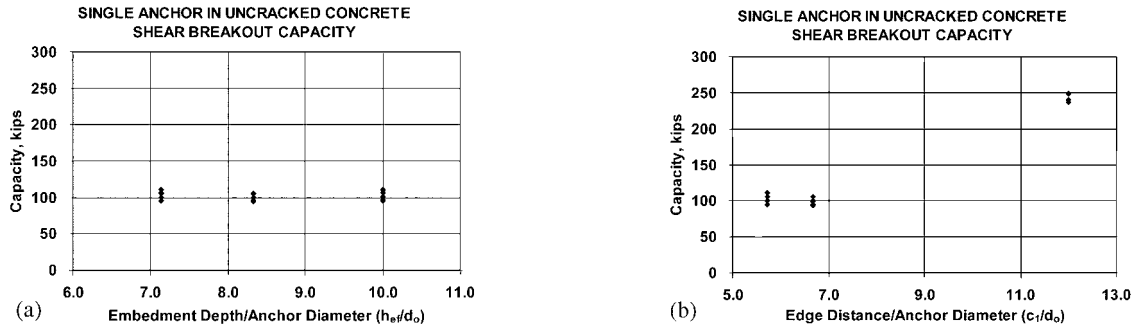

Fig. 9—Tested shear breakout capacities with: (a) h_{ef}/d_o; and (b) c_1/d_o. (Note: 1 kip = 4.448 kN.)

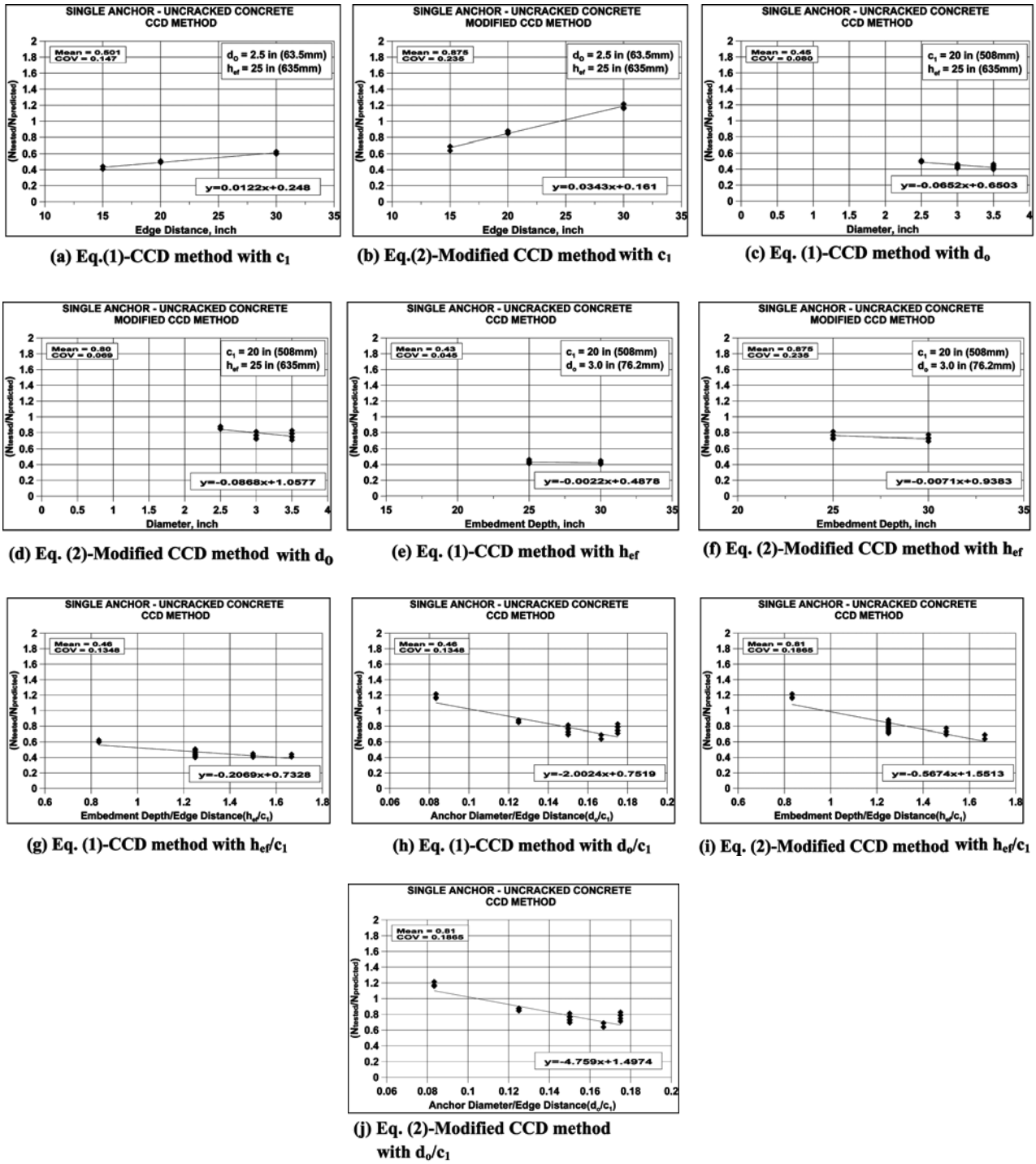

Fig. 10—Ratios of tested-to-predicted concrete shear breakout capacities as function of various parameters.

measured in test Specimens S1 to S7 are plotted as a function of ratios of embedment depth to anchor diameter (h_{ef}/d_o) and edge distance to anchor diameter (c_1/d_o).

EVALUATION OF TEST RESULTS FOR SPECIMENS S1 THROUGH S7 (NO SUPPLEMENTARY REINFORCEMENT)

For Specimens S1 through S7 (no supplementary reinforcement), shear breakout capacities are not influenced significantly by embedment depth or anchor diameter, but are significantly influenced by edge distance (refer to Fig. 9). This implies that in the shear breakout equation of the CCD method, the load bearing length (ℓ), and the anchor diameter (d_o) should have upper limits. In references[7,8] a limit $h_{ef}/d_o = 8$ is proposed, but the shear breakout capacities on headed anchors with large diameters and deep embedments appeared not to be increased with increasing from a ratio of $h_{ef}/d_o = 7.14$ to $h_{ef}/d_o = 10.0$ (refer to Fig. 9). Therefore, a limit of $h_{ef}/d_o = 7$ is proposed for headed anchors with large diameters and deep embedments instead of $h_{ef}/d_o = 8$.

For all prediction equations, most ratios of tested to predicted capacities are less than 1.0 (unconservative), implying that existing methods are unsuitable for the anchors of this study. For ACI 349-97 (a 45-degree cone model), the average ratios of tested to predicted capacities are only approximately 50%, and this value is almost uniform over the ranges of parameters tested (Table 3). For the CCD method, the average ratio of tested to predicted capacities is also only approximately 50% (Table 3), and increases with increasing edge distance (Fig. 10(a)). The main reason for this is that according to Eq. (1), for a constant ratio of embedment depth to anchor diameter, capacity increases in proportion to $\sqrt{d_o}$, and for an embedment depth, capacity increases in proportion to $d_o^{0.3}$, while tests show no such increase with increasing in anchor diameter. Note that in the CCD method,[7,8] the values of d_o and of the ratio h_{ef}/d_o to be inserted in Eq. (1) are limited to $d_o = 1$ in. (25 mm) and $h_{ef}/d_o = 8$, respectively. If those limits are imposed, the average ratio of tested to predicted capacity increases to approximately 0.8—still slightly unconservative.

Using ACI 349-06, but without limiting d_o and h_{ef}, the ratios increase by approximately 15% compared to the CCD method because in ACI 349-06 a ratio of 5% fractile to mean value of 0.75 is assumed as previously mentioned, while in the test this ratio is, on average, 0.85. The modified CCD method, in contrast, agrees much better with the test results, giving an average ratio of 0.83 (Table 3). These ratios increase with increasing edge distance (Fig. 10(b)), and are almost independent of embedment depth and anchor diameter. They decrease with an increasing ratio of embedment depth to edge distance (Fig. 10(i)) and increasing ratio of anchor diameter to edge distance (Fig. 10(j)). This is mainly because the failure load is underestimated for a large edge distance (small ratio of diameter to edge distance) and overestimated for small edge distances (large ratio of diameter to edge distance). Altogether, the influence of these parameters is overestimated in the prediction equation. With proper modification, Eq. (2) can safely be used to design large anchor bolts.

The CCD method, developed for small anchors, overestimates the capacity of large anchors. Equation (2), modified from the CCD method, appears to overestimate the capacity of large anchors at relatively small edge distances to a lesser degree than the CCD method, but still underestimates the capacity of large anchors at an edge distance larger than those of Specimens S1 through S6 (refer to Specimen S7 in Table 3).

According to test results, from $c_1 = 15$ in. (381.0 mm) to $c_1 = 30$ in. (762.0 mm), concrete breakout capacity appeared to increase in proportion to c_1^2. Tests and numerical calculations at the University of Stuttgart[2] with anchors up to a diameter of $d_o = 2$ in. (50.0 mm) show, however, that due to the size effect, the concrete edge failure load increases as a function of $c_1^{1.5}$. The experimental results for large anchors appeared not to be systematically expressed as a function of $c_1^{1.5}$. The exponent on the edge distance term in the CCD equation, therefore, may need to be increased for large anchors, but available experimental results for relatively large sized anchors are very limited to find a proper exponent. Therefore, Eq. (2) is modified by limiting d_o to 2 in. (50.0 mm) and h_{ef} to $7d_o$ (= 14 in. [355.6 mm]) in this paper. The results for $c_1 = 15$ in. (381.0 mm) of a shortest edge distance tested in this research in

$$V_n = 6.5 \cdot f'^{\,0.5}_{cc} \cdot c_1^{1.5} \quad \text{(N) (in SI Units)} \tag{5a}$$

The ratio between the 5% fractiles ($V_{n,5\%}$) and the mean values ($V_{n,m}$) in the tests described herein varied between 0.81 and 0.94, on average 0.85 (refer to Table 3). In practical applications, this ratio might be somewhat higher. Therefore, a ratio $V_{n,5\%} = 0.8V_{n,m}$ is conservatively assumed. With this we get

$$V_{n,\,5\%}(= V_b) = 5.2 \cdot f'^{\,0.5}_{cc} \cdot c_1^{1.5} \quad \text{(N) (in SI Units)} \tag{5b}$$

Assuming $f_{cc}' = 1.18 \cdot f_c'$, the following is obtained

$$V_n = 7.0 \cdot f'^{\,0.5}_{c} \cdot c_1^{1.5} \quad \text{(N) (in SI Units)} \tag{5a-1}$$

$$V_n = 16.7 \cdot f'^{\,0.5}_{c} \cdot c_1^{1.5} \text{ (lb) (in U.S. Customary Units)} \tag{5a-2}$$

$$V_{n,\,5\%}(= V_b) = 5.6 \cdot f'^{\,0.5}_{c} \cdot c_1^{1.5} \quad \text{(N) (in SI Units)} \tag{5b-1}$$

$$V_{n,\,5\%}(= V_b) = 13.4 \cdot f'^{\,0.5}_{c} \cdot c_1^{1.5} \quad \text{(lb)} \tag{5b-2}$$

(in U.S. Customary Units)

In Table 5, capacities predicted by Eq. (5a) are compared with the measured average failure loads (normalized to $f_c' = 5500$ psi [38.0 MPa]), and also with the 5% fractile capacities.

Table 5—Tested capacities versus those predicted by Eq. (5a) or (5b)

		Edge distance, in. (mm)		
		15.0 (381.0) = $6d_o$	20.0 (508.0) = $8d_o$	30.0 (762.0) = $12d_o$
Mean values (Eq. 5(a))	$V_{n,\,test}$, kips (kN)	60.0 (266.9)*	102.5 (455.9)†	242.0 (1076.0)‡
	$V_{n,\,calc}$, kips (kN)	71.9 (320.5)	110.7 (493.5)	203.5 (906.7)
	$V_{n,\,test}/V_{n,\,calc}$	0.83	0.92	1.19
5% fractiles (Eq. (5b))	$V_{b,\,test}$, kips (kN)	48.8 (217.1)	87.2 (387.9)§	209.7 (932.8)
	$V_{b,\,calc}$, kips (kN)	57.7 (256.4)	88.8 (394.8)	163.3 (725.3)
	$V_{b,test}/V_{b,calc}$	0.84	0.98	1.28

*Test Specimen S6.
†Test Specimens S1 to S4.
‡Test Specimen S7.
§$V_{n,5\%} = 0.85\ V_{n,mean}$.

For an edge distance c_1 = 15 in. (381.0 mm) the proposed Eq. (5b) predicts failure loads that are somewhat unconservative, while for edge distance c_1 = 30 in. (762.0 mm), the prediction according to Eq. (5b) is conservative. The proposed Eq. (5b), however, predicts failure loads well for an edge distance c_1 = 20 in. (508.0 mm). The ratio of the predicted failure loads and the calculated 5% fractile of the failure load is 0.84 for Specimen S6 with an edge distance of $6d_o$ (edge distance 15 in. [381.0 mm] and diameter 2.5 in. [63.5 mm]) and 1.28 for Specimen S7 with an edge distance of $12d_o$ (edge distance 30 in. [762.0 mm] and diameter 2.5 in. [63.5 mm]) (refer to Table 5). Therefore, the proposed formula for large anchor bolts with diameters exceeding 2 in. (50.8 mm) and embedment depths exceeding 25 in. (635.0 mm) would be more accurate with an edge distance in the range of $8d_o$ to $9d_o$ (refer to Table 5). The proposed formula may have a systematic error because the exponent of 1.5 on c_1 may not be representative for large anchors. Further tests are required to reduce or eliminate this systematic error. This minimum edge distance of $8d_o$ on the proposed formula is, however, applicable to practical purposes and safety design.

The angle of the failure shape observed for Specimens S1 to S7 was rather low (≤25 degrees). This means that the characteristic spacing would be approximately $s_{cr,V} = 4c_1$, larger than the value assumed in the CCD method ($s_{cr,V} = 3c_1$). A value of $s_{cr,V} = 3c_1$ is, however, acceptable for design based on the test results with supplementary reinforcement being addressed in the following section because supplementary reinforcement will generally be used in nuclear structures. It is therefore proposed for nuclear power plant design that large anchors that do not have supplementary reinforcement but have an edge distance of $8d_o \sim 9d_o$ be designed for concrete edge failure according to ACI 349-06; however, Eq. (4) should be replaced by Eq. (5b-1) in SI Units and Eq. (5b-2) in U.S. Customary Units with a minimum edge distance of $8d_o$.

EFFECTS OF SUPPLEMENTARY REINFORCEMENT

To evaluate the effects of supplementary reinforcement, the forces taken up by the supplementary reinforcement were calculated using strain-gauge data. As shown in Fig. 8, supplementary reinforcement did increase capacity. The increase, however, was much less than what would have been achieved for complete load transfer to the stirrups on either side of the anchorage (refer to Fig. 11). U-shaped hairpins in contact with the anchor (S9 and S9-1) gave increased capacity, but still less than the capacity of the hairpins calculated based on a yield stress of 60 ksi (420 MPa). This is probably due to the flexibility of the hairpins and to the large displacements of the anchor required to develop complete yield of the hairpins. U-shaped hairpins not in contact with the anchor (S9-2) provided slightly more capacity because the cracking of the concrete between the U-shaped hairpin and the anchor might reduce the shear force in concrete between the edge and anchor. In the tests with supplementary reinforcement, the breakout prism angle averaged approximately 35 degrees other than the unreinforced specimens having the angle less than 25 degrees.

Reinforced Specimen S8

Specimen S8 had supplementary reinforcement consisting of six No. 8 bars with 90-degree hooks, four U-shaped stirrups at the first layer, and three layers of U-shaped hangers around the anchor (refer to Specimen S8 in Fig. 2). The nominal bar areas of 0.20, 0.44, and 0.79 in.^{2} (129.0, 284.0, and 510.0 mm^2) of No. 4, 6, and 8 are used to calculate the capacity of the supplementary reinforcement.

The mean capacity (normalized to 5500 psi [38.0 MPa]) and the sum of the mean forces calculated from the measured strains in the reinforcements using Young's modulus E = 29,000 ksi (20,000.0 MPa) are 202 and 169 kips (898.0 and 752.0 kN), respectively. The mean tested shear breakout strength of the otherwise identical Specimen S6 (but without supplementary reinforcement) was 60 kips (266.0 kN).

Comparing the mean capacities of Specimens S6 and S8, the effective increase in capacity due to supplementary reinforcement is roughly 142 kips (632.0 kN). Spalling of the concrete in the region of the small edge distance occurred in front of the tested anchors. The limited increase of the shear failure load may have been caused by the insufficient anchorage length of the supplementary reinforcement in the breakout body.

Reinforced Specimens S9, S9-1, and S9-2

Specimens S9 and S9-2 had supplementary reinforcement consisting of three No. 8 U-shaped bars surrounding the anchors. In Specimen S9, the U-shaped bars directly contacted the anchor, while in Specimen S9-2, they are slightly separated (refer to Specimens S9 and S9-2 in Fig. 2). Test Specimen S9-1 had supplementary reinforcement consisting of two No. 8 U-shaped bars directly contacting the anchors, and two No. 6 hooked bars placed near the anchor. The nominal areas of No. 6 and No. 8 (0.44 and 0.79 in.^{2} [284.0 and 510.0 mm^2]), respectively, were used for the calculation of forces resisted by the reinforcement. Comparison of the mean tested strengths (normalized) of Specimens S6

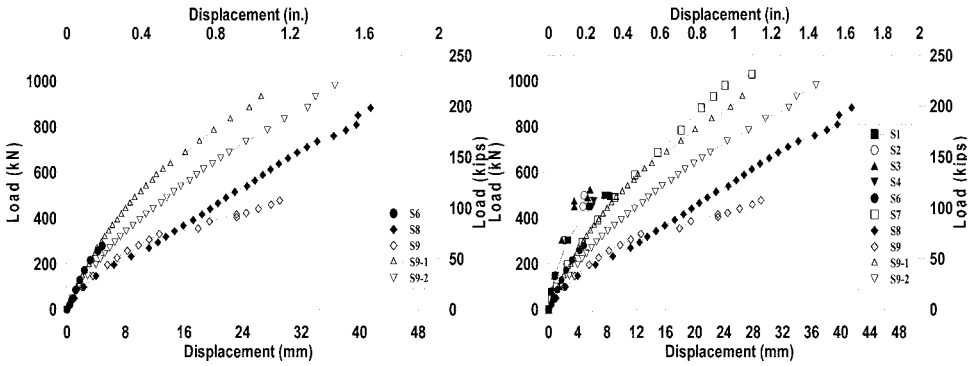

Fig. 11—Influence of supplementary reinforcement on load-displacement behavior.

and S9 shows that the effective increase in capacity due to supplementary reinforcement is roughly 86 kips (382.0 kN). The two No. 8 U-loops were locally yielded at the contact points, but the applied shear was not fully transferred to the concrete. Specimens S9-1 and S9-2, having one replicate, showed the ultimate capacity a little greater than that of Specimen S9 (refer Fig. 8). The test results of S9-1 and S9-2, however, are not included in the comparison of the mean tested strengths because one replicate for Specimens S9-1 and S9-2 was tested only as previously mentioned.

Reinforced Specimen S10

Specimen S10 had supplementary reinforcement consisting of two layers of 2 rods (2-1/2 in. [63.5 mm] in diameter [ASTM A193]) each, with plates 10 x 5 x 2 in. (254.0 x 127.0 x 50.8 mm) (A36) surrounding anchor bolts (refer to Specimen S10 in Fig. 2). The nominal area of one rod (4.9 in.^{2} [3161.3 mm^2]) is used for calculation of the force taken by the rods. The mean tested peak load (normalized to 5500 psi [38.0 MPa]) and the sum of the mean forces calculated from the measured strains in reinforcements and Young's modulus, E, are 109 and 697 kips (484.0 and 3100.0 kN), respectively. The mean tested shear breakout strength of the otherwise identical Specimen S6 (no supplementary reinforcement was 60 kips [266.0 kN], giving an effective increase in capacity due to supplementary reinforcement of approximately 49 kips [217.0 kN]). The rods and plates appeared to not be effective for anchors with a small edge distance.

SUMMARY AND CONCLUSIONS

Shear behavior of large anchors without supplementary reinforcement

The shear breakout capacity of large anchors with diameters exceeding 2 in. (50.8 mm), embedment depths exceeding 25 in. (635.0 mm), and a relatively short edge distance to anchor diameter giving the ratio of c_1/d_o less than approximately 7.0, is overestimated by a factor of approximately 2 by most available formulas, which were developed using data from smaller-diameter anchors. The shear breakout capacities of the tested large anchors with a relatively short edge distance anchor diameter are influenced by edge distance, but not by embedment depth or anchor diameter.

Therefore, in predictive equations based on the CCD method, the load bearing length and anchor diameter should be limited. Proposed equations (5b, or [5b-1], [5b-2]) are recommended for edge distances in the range of $8d_o$ to $9d_o$. As previously mentioned, concrete breakout capacity on large anchors appeared to increase in proportion to c_1^2 and, thus, further tests are required to find the proper exponent on the edge distance term in the proposed equation for large anchors.

The breakout prism angle was rather low (≤25 degrees) and, thus, the characteristic spacing would be approximately $s_{cr,V} = 4c_1$, larger than the value assumed in the CCD method ($s_{cr,V} = 3c_1$). As previously mentioned, however, the value $s_{cr,V} = 3c_1$ should be used in the design of most of structures adopting large anchors with structural supplementary reinforcement.

Shear behavior of large anchors with supplementary reinforcement

Specimens S8, S9, S9-1, and S9-2 had peak capacities more than twice those of otherwise identical specimens without supplementary reinforcement. Therefore, the concrete breakout resistance of anchors with an edge distance $c_1 \geq 15$ in. (381.0 mm) calculated as described previously can be increased by a factor of at least 2.0 if supplementary reinforcement is developed in the remaining concrete having a component parallel to the applied shear around each anchor of an anchor group.

Most shear tests had to be stopped because of limited stroke of the loading actuator before the supplementary reinforcement had been fully mobilized. However, the maximum displacements measured during shear tests do not appear to be small compared to the permissible displacement for such attachments anchored to concrete structures in nuclear power plants. Therefore, it could be judged that there was no need to continue testing to obtain an additional increase in peak loads accompanied by even larger displacements.

The specimen with U-shaped hairpins not in contact with the anchor had slightly greater capacity than those with U-shaped hairpins in contact with the anchor. This was judged as being due to the cracking of the concrete, causing a reduction in the shear force in concrete between the edge and the anchor. However, this is judged from a test of one replicate for Specimen S9-2 and, thus, further test results using more replicates are required to verify this effect. For large anchors with a relatively small edge distance of $6d_o$, the capacity of the supplementary reinforcement was not effectively developed.

ACKNOWLEDGMENTS

The authors acknowledge the financial and technical help of Korea Hydro and Nuclear Power Co. Ltd. and Korea Electric Power Research Institute for financing this research work and also several ongoing research projects related to the capacity of anchorage to concrete structures. The authors are also grateful for the valuable advice of R. Eligehausen (University of Stuttgart), R. Klingner (University of Texas at Austin), and other members of ACI Committee 355, Anchorage to Concrete.

REFERENCES

1. Fuchs, W.; Eligehausen, R.; and Breen, J. E., "Concrete Capacity Design (CCD) Approach for Fastening to Concrete," *ACI Structural Journal*, V. 92, No. 1, Jan.-Feb. 1995, pp. 73-94.

2. Hofmann, J.,"Tragverhalten und Bemessung von Befestigungen am Bauteilrand unter Querlasten mit beliebigem Winkel zur Bauteilkante (Load-Bearing Behaviour and Design of Fasteners Close to an Edge under Shear Loading with an Arbitrary Angle to the Edge)," doctoral thesis, Institut für Werkstoffe im Bauwesen, Universität Stuttgart, 2004, 235 pp. (in German)

3. ACI Committee 318, "Building Code Requirements for Structural Concrete (ACI 318-08) and Commentary," American Concrete Institute, Farmington Hills, MI, 2008, 473 pp.

4. ACI Committee 349, "Code Requirements for Nuclear Safety-Related Concrete Structures (ACI 349-06) and Commentary," American Concrete Institute, Farmington Hills, MI, 2007, 153 pp.

5. ACI Committee 349, "Code Requirements for Nuclear Safety-Related Concrete Structures (ACI 349-97) and Commentary," American Concrete Institute, Farmington Hills, MI, 1997, 123 pp.

6. Lee, N. H.; Kim, K. S.; Bang, C. J.; and Park, K. R., "Tensile Headed Anchor with Large Diameter and Deep Embedment in Concrete," *ACI Structural Journal*, V. 104, No. 4, July-Aug. 2007, pp. 479-486.

7. Eligehausen, R.; Mallée, R.; and Rehm, G., "Befestigungstechnik (Fastening Technique) Betonkalender 1997," Part II, Ernst Sohn, Berlin, Germany, 1997, pp. 609-753.

8. Fuchs, W., "Entwicklung eines Vorschlags für die Bemessung von Befestigungen (Development of a Proposal for the Design of Fastenings to Concrete)," *Report to the Deutsche Forschungsgemeinschaft*, Feb. 1991, 393 pp. (in German)

Disc. 107-S14/From the March-April 2010 *ACI Structural Journal*, p. 146

Shear Behavior of Headed Anchors with Large Diameters and Deep Embedments. Paper by Nam Ho Lee, Kwang Ryeon Park, and Yong Pyo Suh

Discussion by Donald F. Meinheit and Neil S. Anderson

Affiliated Consultant, Wiss, Janney, Elstner Associates, Chicago, IL; Vice President of Engineering, Concrete Reinforcing Steel Institute, Schaumburg, IL

Compliments to the authors for publishing some very unique and needed data on the shear breakout strength of large-diameter and deeply embedded anchors. The discussers are particularly pleased with the conclusion that embedment depth h_{ef} and anchor diameter d_a did not influence the concrete shear breakout strength. This research echoes what the Precast/Prestressed Concrete Institute (PCI) has advocated since the 4th Edition of the *PCI Design Handbook* in 1992 [9]: the concrete shear breakout strength for uncracked concrete was only a function of the concrete compressive strength f_c' and edge distance c_{a1}, that is

$$V_{b,\text{PCI 1992 (design)}} = 12.5\sqrt{f_c'}\,(c_{a1})^{1.5} \quad (6)$$

The form of this equation was further confirmed in an extensive PCI-sponsored research program[10] on welded headed studs used as the basis for both the 6th and 7th Editions of the *PCI Design Handbook*.[11,12] The current 5% fractile shear breakout design equation in the *PCI Design Handbook* and the average equation derived from test data on headed studs embedded in uncracked concrete are, respectively, Eq. (7) and (8)

$$V_{b,\text{PCI 2010 (design)}} = 16.5\sqrt{f_c'}\,(c_{a1})^{1.33} \quad (7)$$

$$V_{b,\text{PCI 2010 (mean)}} = 22\sqrt{f_c'}\,(c_{a1})^{1.33} \quad (8)$$

Further confirmation of the shear breakout equation format being a function of f_c' and c_{a1} was recently presented by Ronald Cook, University of Florida-Gainesville, during an ACI 318 Code meeting.[13] A design (5% fractile) equation for cracked concrete and average strength equation for uncracked concrete applicable for many anchors in shear can be represented by Eq. (9) and (10), respectively

$$V_{b,\text{ACI 2010 (proposed design—cracked)}} = 9.0\sqrt{f_c'}\,(c_{a1})^{1.5} \quad (9)$$

$$V_{b,\text{ACI 2010 (mean—uncracked)}} = 17.0\sqrt{f_c'}\,(c_{a1})^{1.5} \quad (10)$$

The average strength equation (Eq. (10)) was derived from analysis of both cast-in-place and post-installed anchors in normalweight concrete contained in an international database. Equation (10) is a much better concrete strength predictor than the current ACI 318-08[3] Appendix D Eq. (D-25), of which the *mean* value is presented below as Eq. (11).

$$V_{b,\text{ACI 2008 (mean)}} = \left(13\left(\frac{l_e}{d_a}\right)^{0.2}\sqrt{d_a}\right)\sqrt{f_c'}\,(c_{a1})^{1.5} \quad (11)$$

These new test results confirm that a very simple equation, almost identical to that of the tension breakout equation, is accurate for cast-in embedded bolts and headed studs over the full range of anchor diameters.

Korean test data

Because of the importance of the tests reported in the paper, can the authors please report results for each test in each series, along with the corresponding concrete compressive strength? The paper presents only a test series average for the particular variable under consideration. The reference list does not identify another source publication where these test results can be found; therefore, it is important that all tests be adequately documented in the literature for future use.

The actual steel strength of the anchor bolts and reinforcing bars used in the specimens are not reported; the authors only reported minimum strengths corresponding to the specific standard for which the material conformed. Likewise, it is unclear if the anchor bolt threads are included or excluded in the shear plane for these tests. Even though anchor bolt steel strength did not control, actual strengths are necessary parameters for future data analysis.

Discussion of test specimens

Although the researchers took strides to avoid anchor load frame interference, it appears that some tests might be slightly biased due to the provided clear distance between reaction supports. The CCD "mathematical model" purports a $1.5c_{a1}$ spread on each side of the anchor, but unfortunately the concrete "does not know that" and reality dictates this distance should be upward of double that value, $3c_{a1}$, on each side for testing. Support reactions from the test frame can confine the failure surface outer points, which can result in higher failure loads.

Tests in Series S7, the series with the largest spacing between reaction supports, do not appear to be affected by the reaction location. As the load-deflection plots (Fig. 7) indicate, cracking occurred at approximately 22 mm (0.87 in.) where there is a change in slope, and then failure. In the other unreinforced tests with smaller edge distances, the load-deflection plots seem to indicate first cracking at 2 mm (0.08 in.), followed by a line slope change; other deflection readings around 3.5 to 4 mm (0.14 to 0.16 in.) show another line slope change prior to failure. This two-stage slope could be indicative of the restraining effect of the support reactions. Can the authors please comment on this effect, and whether they believe some restraint may have existed due to the shear reaction location?

Our study of Fig. 5 indicates that the failure surfaces in Tests S1-A, S1-C, and S4-E may have been influenced by a corner failure. The shear crack propagation was driven to the

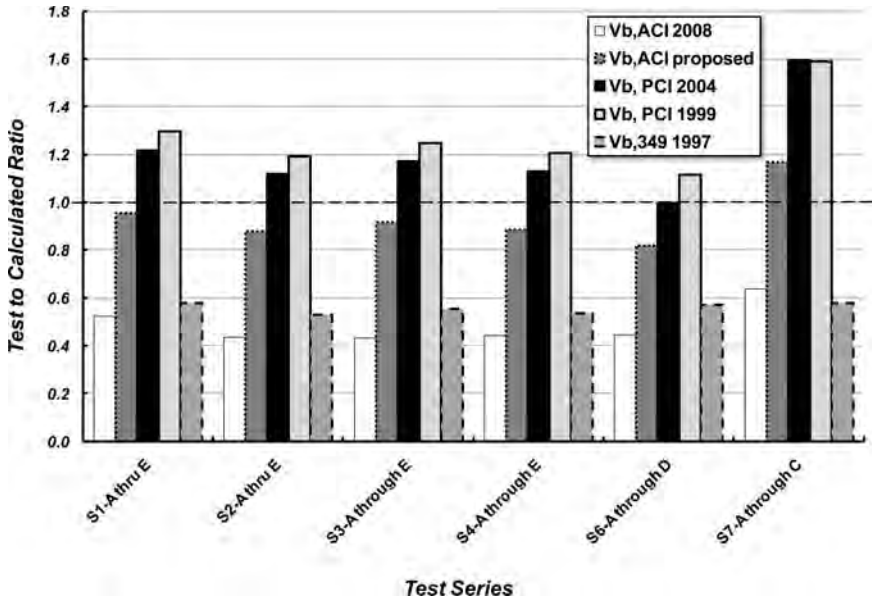

Fig. 12—Test-to-calculated ratios for large-diameter anchors in shear.

specimen edge due to the reaction confining effect. Was this characteristic observed on any other tests, as only six representative tests are illustrated in Fig. 5?

Unreinforced tests

The discussers made comparisons of the various *mean* prediction equations and the tests results for the unreinforced and uncracked concrete tests. Our comparisons shown in Fig. 12 are in terms of test-to-predicted strength ratios. Included in this comparison is the current ACI 318-08[3] Appendix D equation. Clearly Fig. 12 shows the current ACI 318 Appendix D mean equation is unconservative by a significant margin. The equation with the best, closest, fit to these data is the proposed ACI 318, 2010 equation, whereas the PCI equations are conservative predictors of mean strength. The authors should perhaps modify their conclusion to indicate that the design equation for shear breakout in the ACI Code, Appendix D, should be changed to a simpler and better prediction equation.

Anchor reinforcement tests

The provided anchor reinforcement strength exceeded the ACI 318-08 Appendix D mean equation (Eq. (11)). Therefore, there was ample anchor reinforcement in all reinforced tests to carry test loads larger than the concrete cracking capacity load. The reinforced tests can be compared to the results of Series S6 (unreinforced) tests, where d_a, h_{ef}, and c_1 were all the same.

An analysis of Fig. 7(e), representing four tests from Series S6, shows the specimens reached the concrete shear strength when cracks formed at a displacement of approximately 5 mm (0.20 in.). Concrete shear cracking evidence appears in the load-deformation plots for the Series S10 tests, and for some of the tests in Series S8 and S9; cracking is not as evident for Series S8 and S9, perhaps due to the scale of the plots in Fig. 8. It does appear, however, that there is a slope change of the load-deformation plot at approximately 5 mm (0.2 in.) in each case for all tests in Series S8, S9, and S10.

According to Fig. 2, tests in Series S10 had the least amount of anchor reinforcement and reportedly performed the poorest. The Series S10 load-deformation plots clearly show the cracking and transfer of the load to the anchor reinforcing bars. Anchor reinforcement was directly adjacent to and in contact with the embedded anchor loaded in shear; that is, there was no intentional concrete between the anchor and the anchor reinforcement, as in Series S8 and some of the tests in Series S9. In Series S10, the reinforcement bearing plate was located 6 in. (152 mm) below the concrete surface. Although not shown, this location was likely below the shear crack path initiating at the anchor-concrete surface juncture. The tests in Series S8 had the highest capacity, likely attributed to the embedded anchor being confined within a reinforcing bar cage, well-distributed across the failure surface.

Series S9 test behaviors are most interesting. All Series S9 tests had about the same amount of anchor reinforcement, but the reinforcing bar placement is very informative. Specimen S9-2 had hairpin reinforcement not contacting the embedded anchor, whereas all of the anchor reinforcement was in contact with the embedded anchor in S9-A through D. Test S9-2 performed better by having a higher ultimate load and greater stiffness throughout the test (refer to Fig. 8(b)). A companion test, Test S9-1, had two hairpin bars in contact with the embedded anchor, supplemented with two hooked bars closest to the surface and not in contact with the embedded anchor. Specimen S9-1 shows the greatest stiffness and almost the same ultimate strength as Specimen S9-2.

From these anchor reinforcing tests, the discussers conclude the anchor reinforcement may not have to be in direct contact with the embedded anchor, and anchor reinforcing bars near the concrete surface are more effective than deeper embedded bars.

Another conclusion drawn from these tests is the anchor reinforcements may not be 100% efficient, because they were not able to fully develop the anchor reinforcement strength. In each anchor reinforcing test, however, the reinforcement carried the shear load once the concrete cracked. In each case, the reinforced specimens were able to carry at least twice the failure load of unreinforced specimens

in Series S6. For Specimen S10, the capacity may have been greater had the bearing plate assembly been located higher, within the shear failure wedge of concrete. These are significant conclusions drawn by the discussers from this research, which have not been previously discussed.

REFERENCES

9. Precast/Prestressed Concrete Institute (PCI), *PCI Design Handbook*, 4th Edition, PCI MNL 120-92, Chicago, IL, 1992.

10. Anderson, N. S., and Meinheit, D. F., "A Review of the Chapter 6 Headed Stud Design Criteria in the 6th Edition PCI Handbook," *PCI Journal*, V. 52, No. 1, Jan.-Feb. 2007, pp. 84-112.

11. Precast/Prestressed Concrete Institute (PCI), *PCI Design Handbook*, 6th Edition, PCI MNL 120-04, Chicago, IL, 2004.

12. Precast/Prestressed Concrete Institute (PCI), *PCI Design Handbook*, 7th Edition, PCI MNL 120-10, Chicago, IL, 2010.

13. ACI Subcommittee 318-B, Committee correspondence from Ronald A. Cook, University of Florida-Gainesville, proposed code changes for shear breakout of anchors, 2010.

AUTHORS' CLOSURE

The authors would like to thank the discussers for their support of the authors' conclusions and their insightful and constructive discussion to provide the authors an opportunity to further clarify the findings of the experimental study. As the title of the paper implies, the focus was on the concrete shear breakout strength of anchors with large diameters, deep embedments, and relatively short edge distance to anchor diameter. This focus was stated in the research significance section, detailed in the main body of the paper, and reiterated in the summary and conclusions section. The objective of the paper was neither to newly develop nor validate the existing formulas in the current code provisions for anchors with relatively smaller diameter and shallower embedments than those tested in this research.

The discussers indicated that the concrete shear breakout strength for uncracked concrete was only a function of the concrete compressive strength f_c' and edge distance c_{a1}, as the Precast/Prestressed Concrete Institute (PCI) has advocated. The authors have presented that the embedment depth h_{ef} and anchor diameter d_a influence the concrete shear breakout strength, but limited to $h_{ef}/d_a = 7$ for the concrete shear breakout strength of the headed anchors based on the test results with diameters d_a exceeding 2.5 in (63.5 mm), embedment depths h_{ef} exceeding 25 in. (635.0 mm) and $h_{ef}/d_a = 7.14$ to 10.0. It is beyond the scope of this paper to discuss if this research echoes what the Precast/Prestressed Concrete Institute (PCI) has advocated. More tests with various ratios of h_{ef}/d_a less than 7.0 proposed in this paper are therefore required to fully support the discussers' conclusion that embedment depth h_{ef} and anchor diameter d_a did not influence the concrete shear breakout strength irrespective of anchor diameter, embedment depth, and edge distance.

Korean test data

The concrete breakout capacity for each test in each series is shown in Fig. 7—Measured load-displacement relationship (no supplementary reinforcement), and Fig. 8—Measured load-displacement relationship (supplementary reinforcement). The concrete breakout capacity for each test in each series and the corresponding concrete compressive strength were eliminated from this paper due to the limitation in length because they are judged not to be necessary for this paper. The test results were presented in a report in the Korean language as proprietary material of the sponsors.

This research is intended to evaluate the shear concrete breakout capacity for anchors with large diameters and deep embedments. Thus the test specimens are intentionally designed not to induce steel anchor bolt failure but to induce concrete shear breakout failure. Therefore, the actual strengths of individual steel anchor bolts, which are generally greater than nominal strength, were not necessary to be measured for these tests. All of the test specimens in this research, however, used the certified anchor bolt material of ASTM A540, equivalent to ASME SA 540 Grade B23 Class 2 supplied for Korean nuclear power plants.

Discussion of test specimens

The load increment of about 5.5 kips (24.5 kN) after deflection readings around 3.5 to 4 mm (0.14 to 0.16 in.) is approximately 5% of peak load. The displacements at the last load increment were measured at every 1 minute for the first 5 minutes and at every 5 minutes for the next 20 or 25 minutes. Test results show the displacements during the last load increment are increased almost linearly from the previous load increment for around 20 minutes and increased steeply after 20 minutes; that is, no abrupt slope change occurred after deflection readings of around 3.5 to 4 mm (0.14 to 0.16 in.) at peak load for around 20 minutes. The displacements at peak load shown in Fig. 7 are those observed at 25 or 30 minutes, that is, the displacements increased steeply without load increment. From these observations, the authors judged that there were no restraining effects of the support reactions on the peak loads considered as failure loads in this research; however, the displacements obtained from some of the specimens at peak loads were driven by shear crack propagation to the support location. This is an indication that there could be a little restraint effect due to support reactions.

Unreinforced tests

The current ACI 318 Appendix D equation is for small-sized anchors with diameters not exceeding 2 in. (50.8 mm) and embedments depth not exceeding 25 in. (635.0 mm). Therefore, it is beyond the scope of this paper to discuss the current ACI 318 Appendix D equation for small-sized anchors with the findings based on the anchors with large diameters and deep embedments used in this research.

Anchor reinforcement tests

The authors had presented the comparisons of the test results for reinforced test specimens and the results of Series S6 (unreinforced) tests as illustrated in Table 4 and Fig. 11. Based on these test results, the discussers suggested that the anchor reinforcement may not have to be in direct contact with embedded anchor. However, the authors would be careful in making such conclusions because the number of test specimens of S9-2 is very limited. Nevertheless, the authors think that the discussers' feedback on the test results of the anchors reinforced with various types of supplementary reinforcements provide more objective and insightful views on the authors' reinforced test results and that their conclusions will be very useful for practical application as well as for the authors' evaluation and conclusions.

Disc. 107-S27/From the May-June 2010 *ACI Structural Journal*, p. 282

Crack Width Estimation for Concrete Plates. Paper by H. Marzouk, M. Hossin, and A. Hussein

Discussion by Andor Windisch

ACI member, PhD, Karlsfeld, Germany

Assessing different national and international code formulas for prediction of the crack width estimations for thick concrete slabs, the authors recommend a modified numerical model based on the tension chord method.

Regarding Eq. (5) and (6) of the Norwegian Code and considering the possible scatters of the different terms in these both formulas reveals that the ratio 1.7 between the maximum characteristic versus average crack width, w_k/w_m, must rely mostly on the ratio of the crack spacings. It should be also mentioned that the crack width is not the sum of the slips between reinforcing steel and concrete within one crack spacing, but is the result of the slips of same algebraic sign on both sides of this crack (within $l_{s,max}$; refer to the CEB-FIP (1990) Code), even if the crack distance is easily measured and the other lengths are not. The maximum crack distance and the maximum slip length are neither interrelated nor similar to each other. Moreover, it can be shown that the average values of crack distance and crack width are quite insensitive to all influencing factors, such as concrete strength, bond properties, and mode of failures. To estimate the influence of these factors on crack width, the maximum values must be considered.

Similarly, the formula (Eq. (7)) for the average crack spacing according to CSA-S474-04 must be questioned as well: the maximum crack spacing (or maximum slip length) cannot come to $1.7 \times 2.0(C + 0.1S) + 1.7k_1k_2d_{be}h_{ef}b/A_s$, as none of the incorporated parameters have such a high scatter that could result in the factor 1.7.

Considering the test specimens, it should be mentioned that the 25 mm (1 in. or No. 8) bar diameter are definitely too thick relative to the slab thickness (200 mm [8 in.]), in particular in the case of 60 mm (2.4 in.) concrete cover. It is reasonable to limit the bar diameter to $h_{ef}/10$. As mentioned previously, experimental results of the average crack width do not allow for any conclusion.

The authors report that CEB-90 underestimated the maximum crack width by 75%. It could be possible that their calculation was erroneous. In terms of Eq. (10), the authors define ε_{sr2} as the steel strain at a crack. Specifically, it is the steel strain in a crack at cracking load.

Equation (15), related to the modified tension chord model, yields the average crack width. Nevertheless, in Table 3, characteristic values are given: how were these values calculated? Figures 14 and 15 refer to maximum crack widths, whereas Fig. 16 and 17 refer to crack width only, although the experimental values shown are identical with those in Fig. 14 and 15. Which steel stress f_s was chosen as the "end of serviceability limit?"

AUTHORS' CLOSURE

The authors thank the discusser for his interest in the paper and his request for clarification on some aspects of the experimental investigation and the analytical model reported. The discusser is arguing that the ratio 1.7 between the maximum characteristic versus average crack width, w_k/w_m, (Eq. (5) and (6) of the Norwegian Code) must rely mostly on the ratio of the crack spacing.

This argument is not true in the case of two-way slabs with bar spacing less than 300 mm (12 in.). First of all, it should be noted that the characteristic crack width, w_k, is a design value given by codes. Test results of more than 120 two-way slabs (Hossin and Marzouk [2008]; Nawy [1968, 2001]; Nawy and Blair [1971]; Rizk and Marzouk [2010]) showed that the flexural cracks are generated in two orthogonal directions as an image of the reinforcement when the spacing of intersections of the bars or wires, termed as the grid nodal points, is such that the nodal points' spacing does not exceed approximately 300 mm (12 in.). This means that the ratio of 1.7 is not a reflection of the scatter of the ratio of the crack spacing on the characteristic crack width. There are three major factors that contribute to the crack width in a reinforced concrete flexural member: strain release in the concrete in the vicinity of the crack; relative slip between concrete and steel; and distance from the neutral axis.

The discusser is arguing that the maximum crack distance $l_{s,max}$ (CEB-FIP 1990 Code) and the maximum slip length are neither interrelated nor similar to each other. The CEB-FIP technique considers the mechanism of stress transfer between the concrete and reinforcement to estimate crack width and spacing. Prior to cracking, applied tensile load causes equal strains in the concrete and steel. The strains increase with increasing load until the strain capacity of the concrete is reached, at which point cracks develop in the concrete. At the crack locations, the applied tensile load is resisted entirely by the steel. Adjacent to the cracks, there is slip between the concrete and steel, and this slip is the fundamental factor controlling the crack width. The slip causes transfer of some of the force in the steel to the concrete by means of interracial stress (called bond stress) acting on the perimeter of the bar. Therefore, the concrete between the cracks participates in carrying the tensile force.

In the CEB-FIP approach, the crack width is related to the distance over which slip occurs and to the difference between the steel and concrete strains in the slip zones on either side of the crack. It is recognized that cracking is a probabilistic process; therefore, the estimated width is a characteristic crack width, having a low probability of being exceeded. According to this bond-slip model, intermediate cracks can occur only when the spacing between cracks exceeds $l_{s,max}$. Thus, crack spacing will range from $l_{s,max}$ to $0.5l_{s,max}$. The average crack spacing is taken to be approximately 2/3 of $l_{s,max}$.

Once again, the discusser is arguing that Eq. (7) for the average crack spacing according to CSA-S474-04 must be questioned as well, and the maximum crack spacing (or maximum slip length) cannot come to $1.7 \times 2.0(C + 0.1S) + 1.7k_1k_2d_{be}h_{ef}b/A_s$, as none of the incorporated parameters have such a high scatter that could result in the factor 1.7. The argument is not correct for the current experimental test results, as all test specimens presented in the experimental

work have bar spacing less than 250 mm (10 in.) and the evidence of the experimental work showed that the flexural cracks developed in two orthogonal directions as a reflection of the reinforcement grid. Therefore, to control cracking in two-way slabs, the major parameter to be considered is the reinforcement spacing in two perpendicular directions. Research work by Frosch (1999) that was implemented later in the ACI 318-05 Code, abandoned the concept of crack width calculations to control cracking and replaced it with bar spacing limitation. Hence, the experimental results of the average crack width and, consequently, research conclusions, are valid.

The discusser is arguing that the 25 mm (1 in. or No. 8) bar diameter is definitely too thick relative to the slab thickness (200 mm [8 in.]), in particular in the case of 60 mm (2.4 in.) concrete cover. It is reasonable to limit the bar diameter to $h/10$.

It should be noted that this slab was designed considering the maximum capacity of the test frame limitation. The argument could be considered valid for building slabs and it is reasonable to limit the bar diameter to the empirical value ($h/10$). The argument may not be valid, however, for offshore concrete structures applications, which is the main objective of the presented research work, where large bar diameters and thick concrete covers are common practice for such structures. For example, in the case of the Atlantic Oil platform (Hibernia Offshore NFLd), the ice wall thickness was 400 to1000 mm (16 to 40 in.) and it was reinforced with 55 mm (2.16 in.) diameter bar in several layers.

Regarding the statement of the crack width values that were estimated using CEB-FIP 1990 Code formula is underestimated by 75%, this is a typographical error and the reference should be related to the Eurocode (EC 2) 2004 only—not to the CEB-FIP 1990 Code. For the list of references, the fourth reference on p. 290 should read "CEN Eurocode 2 (EC 2) 2004-1-1, 2004, "Design of concrete....." and not as "BS EN 1992-1-1:2004 Design of concrete.." The corrected reference is given in this closure's References section.

The crack width values given in Table 3 were calculated using Eq. (15) related to the modified tension chord model and were multiplied by 1.7 to yield the characteristic crack width values. The word "maximum" should be added to the titles of Fig. 16 and 17.

The steel stress f_s was chosen according to the ACI 318-08 Code limit. ACI 318-08, Section 10.6.4, allows the value of f_s at service loads to be taken as $0.67f_y$. This value represents the ratio between service loads and the average factored loads on a structure. The assumption of $f_s = 0.67f_y$ is based on Gegely and Lutz (1968) formula; f_s is the calculated stress in reinforcement at service load, which equals the unfactored moment divided by the product of steel area and internal moment arm.

REFERENCES

CEN Eurocode 2 (EC 2) 2004-1-1, 2004, "Design of Concrete Structures—Part 1-1: General Rules and Rules for Buildings," Comite Européen de Normalisation (CEN), Brussels, 230 pp.

Hossin, M., and Marzouk, H., 2008, "Crack Spacing for Offshore Structures," *Canadian Journal of Civil Engineering*, V. 35, No. 12, pp. 1446-1454.

Nawy, E., 1968, "Crack Control in Reinforced Concrete Structures," ACI JOURNAL, *Proceedings* V. 65, No. 10, Oct., pp. 825-836.

Nawy, E., 2001, "Design for Crack Control in Reinforced and Prestressed Concrete Beams, Two-Way Slabs and Circular Tanks," *Design and Construction Practices to Mitigate Cracking*, SP-204, F. G. Barth and R. Frosch, eds., American Concrete Institute, Farmington Hills, MI, pp. 1-42.

Nawy, E., and Blair, K., 1971, "Further Studies on Flexural Crack Control in Structural Slab Systems," *Symposium on Cracking, Deflection and Ultimate Load of Concrete Slab Systems*, SP-30, R. E. Philleo, ed., American Concrete Institute, Farmington Hills, MI, pp. 1-32.

Rizk, E., and Marzouk, H., 2010, "A New Formula to Calculate Crack Spacing for Concrete Plates," *ACI Structural Journal*, V. 107, No. 1, Jan.-Feb., pp. 43-52.

Disc. 107-S32/From the May-June 2010 *ACI Structural Journal*, p. 330

Shear Strengths of Prestressed Concrete Beams Part 1: Experiments and Shear Design Equations. Paper by Arghadeep Laskar, Thomas T. C. Hsu, and Y. L. Mo

Discussion by Andor Windisch

ACI member, PhD, Karlsfeld, Germany

The authors report on five full-scale prestressed I-beams and present a new equation for the shear strength of prestressed concrete beams. This new equation is a function of the shear span-depth ratio (a/d), the square root of strength of concrete ($\sqrt{f_c'}$), the web area ($b_w d$), and the transverse steel ratio (ρ_t).

The discusser has the following question: How does the prestressing influence the shear strength? The authors refer to the results of Lyngberg (1976) where the prestressing force does not have significant effect on the shear capacity. This statement appears erroneous. The test results of Lyngberg show a very clear and pronounced influence of the effective prestressing force (N_∞) on the concrete contribution V_c. The concrete contribution V_c increased linearly by $0.12N_\infty$. This ratio corresponds to the results of other researchers; thus, the design expressions proposed by the authors should be corrected accordingly.

Beams B1 to B3 were in the shear valley of Kani (1964), which means that the ultimate shear load increases quite dramatically as the shear span-depth ratio decreases, beginning at $a/d \approx 2.5$, which was the case here. Nevertheless, in the case of Beams 4 and 5 ($a/d > \sim 3.5$), the span-depth ratio may not influence the contribution of concrete in shear, V_c, any more (refer to Fig. 9). Another point may be made that, in the case of small shear span-depth ratios, the longitudinal size of the support, and loading plates, respectively, influence the inclination of the kinematically possible failure surface; hence, a/d is not the prominently effective geometrical influencing factor.

The authors refer to Laskar et al. (2006) for the argument that the shear strength would not be significantly affected by

Table 2—Shear failures in Lyngberg's prestressed specimens

Specimen	Concrete strength, MPa	Stirrup strength, kN	Prestress, kN	$V_{u,test}$, kN
2A-3	32.6	62.2	631	506
2B-3	33.9	64.9	629	515
3A-2	31.1	67.0	421	489
3B-2	27.5	63.1	421	433
4A-1	31.5	64.5	217	469
4B-1	30.4	66.5	209	454

the angle of failure plane. This statement is correct in the case of shear span-depth ratios greater than ~3.5 only. In fact, the *a*/*d* ratio introduced by the authors refers to the angle of failure plane.

The concept of Loov (2002), taking into account the rational number of stirrups crossing the failure crack instead of calculating with smeared stirrups is, in principle, correct and progressive. Nevertheless, in the case of beams with small shear span-depth ratios (< 2.5), Eq. (3) and Fig. 8 should be corrected. In those cases, the inclination of the failure plane is less than 45 degrees.

AUTHORS' CLOSURE

Table 2, taken from Lyngberg (1976), shows how the level of prestress influences the ultimate shear strength. It can be seen that concrete strength has more effect than the prestress force on the ultimate shear strength. Lyngberg stated in his Conclusion 2, "The effect of prestress does not seem to contribute *significantly* to the *ultimate* shear resistance." This conclusion appears to be correct when the effective prestress force varies from 60% to 40% of the tensile strength of the flexural reinforcement. Sixty percent is typically "full prestress," and 40% is about 1/3 replacement of prestressed strands by mild steel. However, when the effective prestress force is less than 40% of the tensile strength of the flexural reinforcement and is approaching zero, the ultimate shear forces could decrease significantly.

The physical meaning is clear: When the web is uncracked under large effective prestress, the entire web area $b_w d$ is effective in resisting the ultimate shear. When the web is cracked under small effective prestress, however, only the uncracked compressive web area is effective in resisting ultimate shear. A recent study shows that in the case of reinforced concrete beams with zero prestress, c is the depth of the compression zone and is expressed by $c/d = (\sqrt{2\rho_w n + (\rho_w n)^2} - \rho_w n) \cdot \rho_w$ is the longitudinal steel ratio, and n is the modulus ratio E_s/E_c.

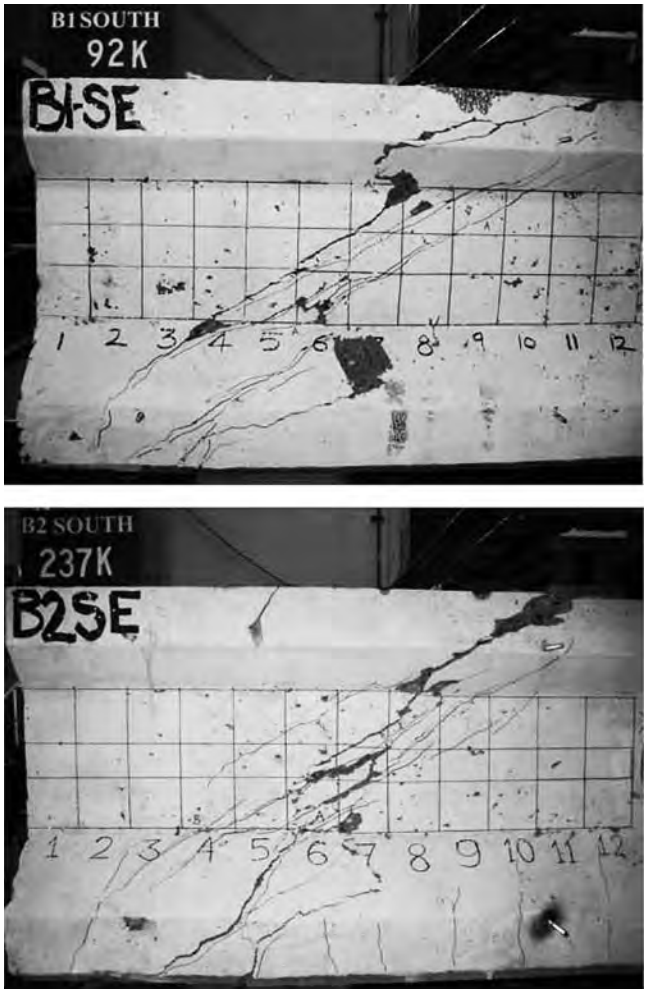

Fig. 13—Forty-five-degree crack patterns of Beams B1 and B2 showing web-shear failure.

Figure 9 shows that the *a*/*d* ratio still affect V_c when it is in the range greater than 3.5. Specimens by Hernandez (1958), Mattock and Kaar (1961), and Elzanaty et al. (1986) show a decrease in the contribution of concrete in shear V_c when the *a*/*d* ratio is greater than 3.5.

Specimens with *a*/*d* ratios less than 3.5 were also observed to fail along a 45-degree inclined plane, as shown in Fig. 13. Specimens with *a*/*d* ratios greater than 3.5 were also observed to fail along a 45-degree inclined plane, as shown in Fig. 7 of the paper. It can be concluded that the shear strength is not significantly affected by the angle of failure plane.